journal

J. Am. Ceram. Soc., 99 [1] 27–34 (2016)
DOI: 10.1111/jace.13930

A Novel One-Step Flame Synthesis Method for Tungsten-Doped CCTO

Laxman Singh,[‡] Byung Cheol Sin,[‡] Ill Won Kim,[§] K.D. Mandal,[¶] Hoeil Chung,[‖] and Youngil Lee[‡,†]

[‡]Department of Chemistry, University of Ulsan, 93 Daehak-ro Nam-gu, Ulsan 680-749, Korea

[§]Department of Physics, University of Ulsan, 93 Daehak-ro Nam-gu, Ulsan 680-749, Korea

[¶]Department of Chemistry, Indian Institute of Technology, Banaras Hindu University, Varanasi 221005, Uttar Pradesh, India

[‖]Department of Chemistry, Hanyang University, Haengdang-dong17, Seongdong-Gu, Seoul 133-791, Korea

An efficient synthesis is used for the first time to prepare $CaCu_3Ti_{4-x}W_xO_{12}$ (x = 0.01, 0.03, and 0.05) electroceramics for energy storage capacitors. $CaCu_3Ti_{4-x}W_xO_{12}$ ceramics are synthesized via flame synthesis of metal nitrates precursors in nonaqueous solution using cheap, stable, and insoluble solid TiO_2 powder. The pathway yielded a $CaCu_3Ti_4O_{12}$ (CCTO) phase with the traces of CuO and $CaTiO_3$ sintered at 1050°C for 30 h. The SEM micrograph shows the grains with smooth surfaces associated with cubical appearance and the size range of 1.5–7, 2.0–7.5, and 2.0–8.0 μm for CCTWO01, CCTWO03, and CCTWO05, respectively. The EDX and XPS analyses show the presence of Ca, Cu, Ti, W, and O elements confirming the purity of these ceramics. The complex impedance and modulus (M) spectroscopy show that the dielectric constant (ε_r) values of the W-doped CCTO were dominantly affected by the electrical properties of the grain boundary, which is also evident from the SEM micrographs. The grain-boundary resistance decreased with increasing tungsten content. The activation energies for the grain boundaries were calculated from the impedance and modulus data using the slope of the ln τ versus $1/T$ and were found to be in the range 0.62–0.67 eV.

I. Introduction

In the last decade, ABO_3 (where A and B are cations of different sizes (A larger than B) and O is the anion) type oxides materials have received wide attention owing to their importance and potential impact in ceramic capacitor, dynamic random access memory, transducers, microelectronic, microwave device applications, and other electronic devices.[1–4] Among, calcium copper titanate, $CaCu_3Ti_4O_{12}$ (CCTO), belonging to ABO_3 family with a high dielectric constant is the best choice. CCTO has a pseudo-cubic perovskite structure with the space group of Im3 and the lattice parameter of 7.391 Å.[5–7] CCTO is a promising material for many important industrial applications in microelectronics and memory devices owing to its very high and thermally stable dielectric constant ($\varepsilon_r \approx 10^4$–$10^5$) in the temperature range 100–600 K.[8–10] The dielectric properties of the CCTO have been improved by the various cationic substitutions at Cu or Ti site.[11–18] The cationic substitutions in CCTO significantly affect its dielectric constant, dielectric loss, and electrical properties by controlling the chemistry and structure of the interfacial regions at the grain boundaries. There are two types of substitutions: acceptor and donor. Acceptor cationic substitutions are defined as cations with ionic charges lower than the ions they replace, and donor cationic substitutions are defined as cations with a higher ionic charge than the ions they replace. There are only few reports were found on donor cationic substitutions of Nb^{5+}, Ta^{5+}, and Sb^{5+} at Ti-site in CCTO using conventional solid-state reaction.[19–21] The dielectric properties of CCTO are also strongly dependent on the processing conditions such as preparation routes,[22–24] sintering temperatures,[25,26] and sintering durations.[27,28] Synthesis method of CCTO ceramic has played a significant role in determining the microstructural, electrical, and dielectric properties. Among various preparation routes, the sol–gel route is an easy, simplest, and most efficient route for producing ceramic materials in bulk amounts with excellent scope of microstructural and process control. Several studies based on the sol–gel technique have been reported for the preparation isomorphs of CCTO using an expensive alkoxide, oxynitrate, or chloride of titanium as the titanium source. Although significant progresses have been achieved in the sol–gel techniques, there are a few problems such as Ti source used in these techniques are very expensive, not easy to handle, and extremely sensitive to the environmental conditions such as moisture, light, and heat. In the window of donor cationic substitutions and preparation routes of CCTO, further detailed studies are necessary to better understand its dielectric and electrical properties using appropriate new chemical based routes. To the best of our knowledge, there are no reports on the preparation of tungsten (W)-doped CCTO ceramic using inexpensive solid TiO_2 as a raw material in nonaqueous solvent. The W^{6+}-substituted ceramics obtained by this route were characterized by various physiochemical characterizations along with measurement of their dielectric properties and impedance analysis.

II. Experimental Section

(1) Materials Syntheses

First, an stoichiometry amount of $Ca(NO_3)_2{\cdot}4H_2O$ (97.0%, Daejung), $Cu(NO_3)_2{\cdot}3H_2O$ (99.0%, Junsei, Tokyo, Japan), and H_2WO_4 (99.0%, Junsei) were dissolved in 100 mL 2-methoxyethanol (99.0%, Alfa Aesar, Lancashire, UK) to prepare the $CaCu_3Ti_{4-x}W_xO_{12}$ (x = 0.01, 0.03, and 0.05) ceramics abbreviated as CCTWO01, CCTWO03, and CCTWO05, respectively. Then, stoichiometric amounts of solid TiO_2 (99.0%, Sigma-Aldrich, St. Louis, MO) in solid-state form without any specification of the morphology and particle size equivalent to the metal ions were added to the solution. The stoichiometric amount of reactants and sintering conditions used for the synthesis of CCTWO ceramics are listed in Table I. The resulting dispersion was sonicated for 30 min. The well-dispersed solution was heated on a hot plate using a magnetic stirrer in the temperature range 70°C-90°C to evaporate the organic solvent until the combustion

J. Varela—contributing editor

Manuscript No. 36367. Received February 5, 2015; approved August 5, 2015.
[†]Author to whom correspondence should be addressed. e-mail: nmryil@ulsan.ac.kr

Table I. Experimental Conditions for the Synthesis of $CaCu_3Ti_{4-x}W_xO_{12}$ (x = 0.01, 0.03, and 0.05) Ceramics

Specimen	Concentration of reactants in (g)				Sintering Temp. (°C)	Duration (h)
	$Ca(NO_3)_2.4H_2O$	$Cu(NO_3)_2{\cdot}3H_2O$	TiO_2	H_2WO_4		
CCTWO01	2.4345	7.3212	3.1948	0.1009	1050	30
CCTWO03	2.4345	7.3212	3.1303	0.3028	1050	30
CCTWO05	2.4345	7.3212	3.0657	0.5047	1050	30

flame of the precursor appeared. The ignition process was performed in air by self-propagating flame of metal nitrates, which released a large amount of gases and produced a crude black color powder of CCTWO. Moreover, the proposed method did not require complexant agents as compared with other self-combustion synthesis where the process involves a self-sustained reaction in a homogeneous solution of different oxidizers (e.g., metal nitrates) and fuels (e.g., citric acid, urea, glycine, etc).[29] The obtained combustion powders were then pressed into cylindrical pellets using a hydraulic press and sintered at 1050°C for 30 h in air in an electric furnace.

(2) Instrumentation

XRD measurements (Rigaku Ultima IV, Tokyo, Japan) were performed to investigate the crystal structure of the ceramics using Cu Kα radiation. The morphology of the fractured surfaces of the ceramics was investigated by SEM (Model JEOL JSM7600F, Tokyo, Japan). EDX analyzer (model Inca X-max, Oxford, UK) was used for elemental analysis. XPS analysis was performed using a Thermo Fisher Scientific $K\alpha$ (Waltham, MA) in wide-scan survey mode and high-energy resolution with AlK_α (1486.6 eV). Data concerning the density measurement of sintered CCTWO01, CCTWO03, and CCTWO05 ceramics were measured by the Archimedes method using a pycnometer.[30] For the measurement of dielectric and electrical properties of the CCTWO ceramics the silver paste was applied to both sides of the circular faces of the ceramic pellets and measured using an impedance analyzer (Hioki 3522-50 LCR HiTESTER, Nagano, Japan) in the frequency and temperature ranges of 1–10^5 Hz and 308–500 K, respectively.

III. Results and Discussion

Figure 1 shows the XRD patterns of CCTWO01, CCTWO03, and CCTWO05 ceramics sintered at 1050°C for 30 h. All the diffraction peaks were indexed based on the body-centered cubic unit cell similar to undoped CCTO (JCPDS 75-2188), confirming the formation of a major phase of CCTO besides some secondary phases of CuO and $CaTiO_3$. The small amounts of secondary phases $CaTiO_3$ and CuO appeared. The appearance of secondary phases may be attributed to the (i) pure CCTO phase is only obtained when the ratio of calcium, copper, and titanium is very closed to the stoichiometric one as reported earlier.[31,32] (ii) less solubility of W^{6+} ion in CCTO lattice and (iii) charge neutrality are not maintained by electronic compensation due to the large disparity between the ionic charge of W^{6+} than Ti^{4+} ions.

Figure 2 shows the microstructures of the CCTWO01, CCTWO03, and CCTWO05 ceramics sintered at 1050°C for 30 h, indicating a slight increase in the grain size with increasing W concentration. The SEM images of all the ceramics show a bimodal distribution of the grains. The small grains are distributed among the large grains of few micrometers. The grain size ranges of CCTWO01, CCTWO03, and CCTWO05 ceramics are 1.5–7, 2.0–7.5, and 2.0–8.0 μm, respectively. It is also observed that the microstructures showed the abnormal grain growth. Based on the CuO–TiO_2 phase diagram, a eutectic point was reported at 919°C.[33] Cu-based eutectic melts were formed in the interspace among grains and transforms into the CuO liquid phase during sintering which leads to abnormal grain growth and densification of the ceramics with increasing concentration of tungsten.[34,35] The apparent densities of the CCTWO01, CCTWO03, and CCTWO05 ceramics were found to be 3.86, 3.94, and 4.34 g/cm^3, respectively. It is also clearly observed from the Fig. 2 that the ceramics shows the porous microstructure. The volume fraction porosity of the CCTWO01, CCTWO03, and CCTWO05 ceramics were found to be 0.24, 0.22, and 0.14, respectively. The most significant feature of CCTWO05 microstructure in Fig. 2(c) is that grains are surrounded by the secondary phase of CuO present at the grain boundaries, which is also detected in the XRD pattern. The presence of the CuO phase is mainly because of the Cu 2p diffusion from the inside to the surface of the grains and oxygen missing from the grain boundaries at high temperatures during the sintering process.[36]

To confirm the elemental compositions of CCTWO01, CCTWO03, and CCTWO05 ceramics, the EDX analysis was carried out. The atomic percentages of Ca, Cu, Ti, W, and O in CCTWO ceramics obtained from EDX analysis are listed in Table II and clearly show the presence of Ca, Cu, Ti, W, and O confirming the purity of the ceramics. The grain-boundary EDX analyses of CCTWO05 were also carried out to confirm the presence of CuO and listed data in the

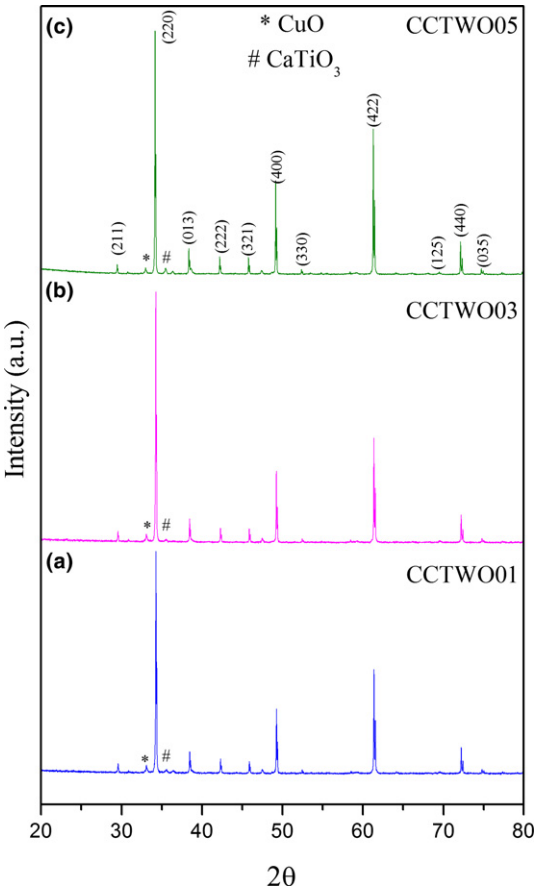

Fig. 1. XRD patterns of (a) CCTWO01, (b) CCTWO03, and (c) CCTWO05 sintered at 1050°C for 30 h.

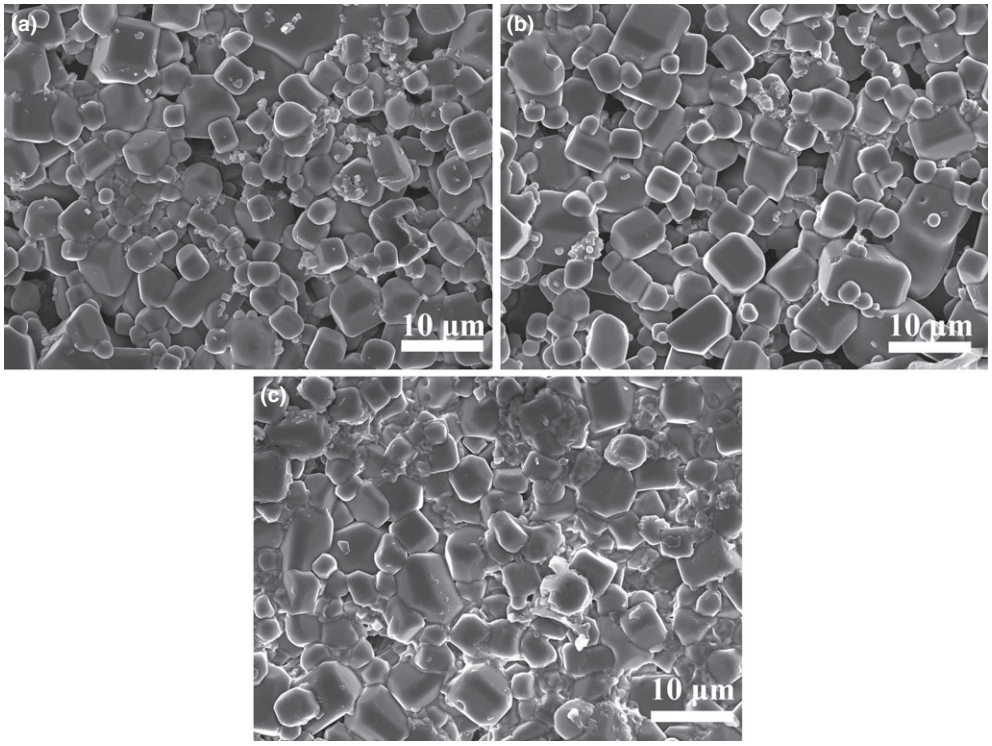

Fig. 2. SEM micrographs of (a) CCTWO01, (b) CCTWO03, and (c) CCTWO05 sintered at 1050°C for 30 h.

Table II. Atomic Percentages of Elements for $CaCu_3Ti_{4-x}W_xO_{12}$ (x = 0.01, 0.03, and 0.05) and $CaCu_3Ti_{3.95}W_{0.05}O_{12}$ in the Grain and at Grain Boundary

	At% of elements				
$CaCu_3Ti_{4-x}W_xO_{12}$	Ca	Cu	Ti	W	O
x = 0.01	5.1	11.3	17.6	0.3	65.7
x = 0.03	5.3	11.8	17.2	0.5	65.2
x = 0.05	4.3	16.6	13.9	0.9	64.3
x = 0.05 (Grain)	4.6	13.6	18.3	0.05	63.4
x = 0.05 (Grain boundary)	0.5	40.6	1.6	0.08	57.2

Table II. It is found that the atomic percentages of the grains of CCTWO05 are in accordance with the stoichiometric ratio of the CCTWO phase. In the case of grain-boundary, EDX data show the secondary phase having up to 33.5% of Cu, percentage, which is much higher than the CCTWO grains along with the existence of W. Combined with the XRD results, the secondary liquid phase was confirmed to be CuO (or rich in CuO). The existence of W in both the grain and grain boundary was clearly detected from the EDX data, indicating that only some of the W^{6+} enters the lattice of the CCTO ceramics and the remainder W atoms may concentrate at the grain boundaries, which may be responsible for the appearance of the secondary phases of CuO and $CaTiO_3$.

Figure 3 shows the representative XPS spectra of CCTWO03 for Ca 2*p*, Cu 2*p*, Ti 2*p*, and W 4*f* metal ions. From the full XPS spectrum in Fig. 3(a), it is clear that only peaks corresponding to Ca, Cu, Ti, W, and O are appeared proving the compositional purity of the ceramic. As shown in Fig. 3(b), the peaks at 346.21 and 349.75 eV are assigned to Ca $2p_{3/2}$ and Ca $2p_{1/2}$, respectively. Figure 3(c) clearly shows the Cu $2p_{3/2}$ and Cu $2p_{1/2}$ spectra at 933.68 and 953.80 eV, respectively, together with satellite peaks on the higher binding energy side which is similar to that earlier reported for Cu^{2+} in $CaCu_3Ti_4O_{12}$.[37] The binding energy positions of both metals are related to the oxidation state, which is agreed well with previous reports.[38] Figure 3(d) shows the XPS pattern of Ti 2*p*. Titanium is in the +4 state, which is evident from the shape and symmetry of the peak. Its binding energy of Ti 2*p* lies in the range 450–470 eV showed two prominent peaks with their positions at 457.93 and 463.73 eV, corresponding to the Ti 2*p* doublet, namely Ti $2p_{3/2}$ and Ti $2p_{1/2}$, respectively.[39,40] The typical doublet W 4*f* peaks, W $4f_{5/2}$ and W $4f_{7/2}$, are clearly visible in the W 4*f* core-level spectra as shown in Fig. 3(e) at 42.80 and 36.38 eV, respectively, and in good agreement with the earlier reports of the W 4*f* XPS spectra with same peaks at +6 oxidation state.[41,42]

Figure 4 shows the variation in the ε_r of CCTWO ceramics as a function of temperature at some fixed frequencies. The ε_r values for the CCTWO01, CCTWO03, and CCTWO05 ceramics at 308 K and 1 kHz were 3145, 4750, and 6022, respectively. Notably, the values of ε_r slightly increases with increasing tungsten concentration toward lower temperature range which may be due to the slightly increasing in the grain size of the ceramics. The dielectric permittivity of the CCTO changes with the modification of the grain size.[43,44] According to the widely accepted internal barrier layer capacitance (IBLC) model, the larger grains size create the greater number of crystal defects than smaller ones, which allows for more internal barrier layers and leads to an increase in the dielectric constant.[45,46] The dielectric behavior can be divided into two regions for all the ceramics. In the temperature region (<400 K), the dependence of ε_r on both the frequency and temperature is very weak, and whereas at the higher temperature region (>400 K), ε_r shows the increasing trend for CCTWO01, CCTWO3 than the CCTWO05 with strong frequency dispersion and temperature dependence. The ε_r is very high at 1 kHz and decreases with increasing frequency at temperatures >400 K. Such a drastic decrease in the ε_r values at higher frequencies can be described in terms of the interfacial space charge polarization,[47] arising from the heterogeneous microstructures. The space charge polarization increases with increasing temperature because of increasing in the dc conductivity. Thus, the interfacial polarization is revealed as a rapid increase in the ε_r at high temperatures and low frequencies.

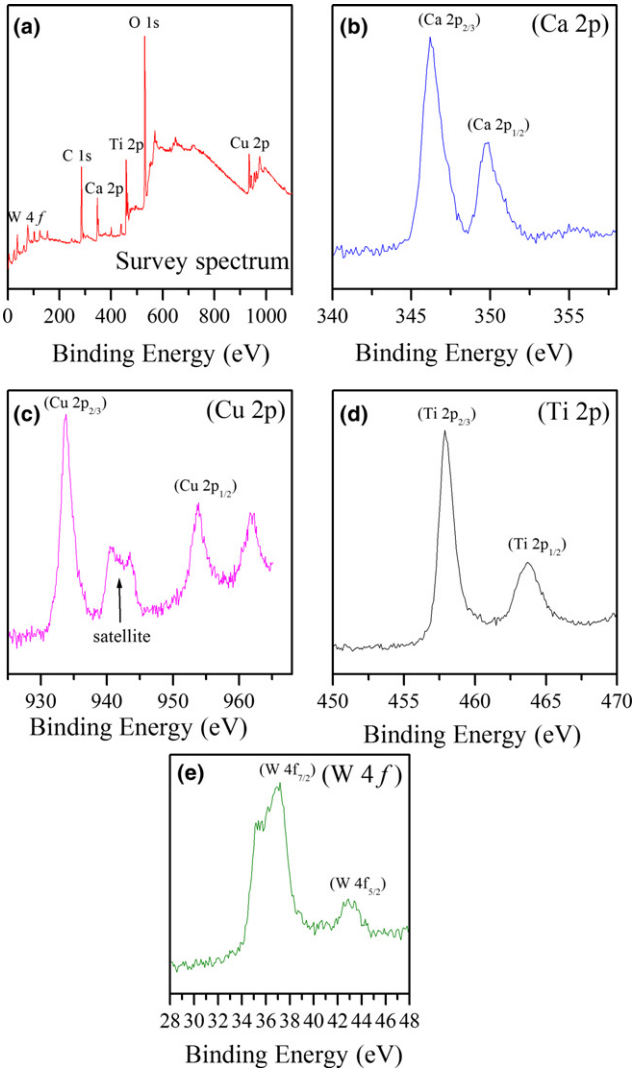

Fig. 3. XPS core-level spectra of (a) survey spectrum, (b) Ca 2*p*, (c) Cu 2*p*, (d) Ti 2p, and (e) W 4 *f* for CCTWO03 sintered at 1050°C for 30 h.

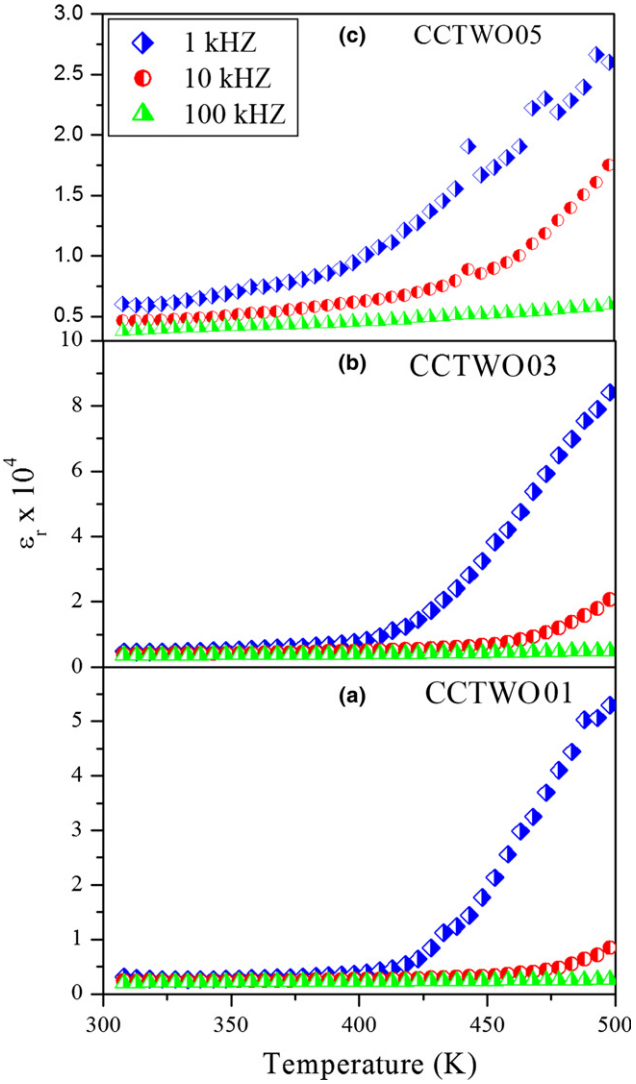

Fig. 4. Variation in the ε_r vs. temperature of (a) CCTWO01, (b) CCTWO03, and (c) CCTWO05 sintered at 1050°C for 30 h at 1, 10, and 100 kHz.

The variation in the dielectric loss (tan δ) of the CCTWO ceramics as a function of temperature at some fixed frequencies is shown in Fig. 5. The values of tan δ for the CCTWO01, CCTWO03, and CCTWO05 ceramics at 308 K and 1 kHz were 0.31, 0.22, and 0.34, respectively. Notably, the overall values of tan δ increase with increasing W concentration at all the measured frequencies. The tan δ was found to be lower at higher frequencies and increased with decreasing frequency and increasing temperature, because of the increase in the conductivity with increasing temperature. Moreover, the values of the dielectric loss factor increase very strongly with increasing temperature (>400 K) with a dielectric relaxation peak in the temperature range 400–450 K at 1 kHz for all the ceramics. This dielectric dispersion is related to a conductivity phenomenon, obeying the Arrhenius-type thermal activation law.

The frequency dependence of the dielectric permittivity and tan δ of CCTWO ceramics at 328 K in the frequency range 10–10^5 Hz are shown in Fig. 6. All the ceramics show high ε_r (>10^4) at the low-frequency region ($f < 10^2$ Hz), and the dielectric permittivity increases with increasing W content over the entire frequency range. The highest permittivity for CCTWO05 was 9.6×10^3 at 100 Hz, whereas only 3.7×10^3 for CCTWO01 ceramic at 100 Hz. In addition, with increasing frequency, the ε_r steadily decreases approaching a constant value at 10^4 Hz.

The frequency dependence of tan δ at 328 K is shown in Fig. 6(b). In the *f* range 10-10^2 Hz, tan δ of all the ceramics were increased rapidly with decreasing frequency, mainly because of the effect dc conduction in the bulk ceramics.[48] At low frequency, tan δ of CCTWO ceramics were increased with increasing *x* from 0.01 to 0.5. When $f > 10^3$ Hz, tan δ of all the ceramics were almost constant. The higher permittivity and loss at the low frequency may be because of the presence of interfacial polarization in these ceramics.[49]

Figure 7(a) shows the AC conductivity, log σ_{AC} versus the reciprocal temperature ($1/T$), measured at 1 kHz for CCTWO01, CCTWO03, and CCTWO05 ceramics, indicating that W doping significantly changed the conductivity (σ_{AC}) and making CCTWO5 ceramic more conductive than CCTWO03 and CCTWO01. The inset of Fig. 7(a) shows the trend of conductivity values of σ_{AC} at 308 K and 1 kHz for $CaCu_3Ti_{4-x}W_xO_{12}$ ($x = 0.01$, 0.03, and 0.05) which seems the similar conductivity behavior to the other materials.[50–57] The results show an increasing trend in σ_{AC} with increasing W concentration in the measured temperature range. The high conductivity of CCTWO5 ceramic is responsible for the high ε_r of this ceramic, which also supports the presence of the IBLC structure. The temperature-dependent σ_{AC} of all the ceramics exhibited the Arrhenius-like behavior.[58] The AC conductivity dependence on the temperature of the ceramic can be defined by the following equation:

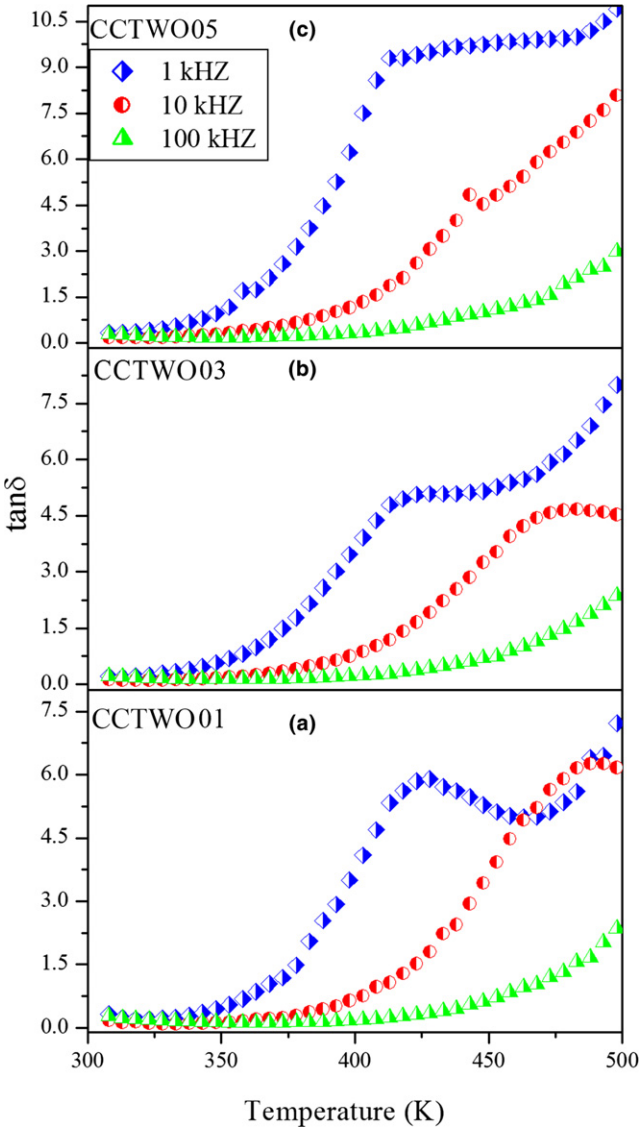

Fig. 5. Variation in dielectric loss (tan δ) vs. temperature of (a) CCTWO01, (b) CCTWO03, and (c) CCTWO05 sintered at 1050°C for 30 h at 1, 10, and 100 kHz.

$$\sigma_{AC} = \sigma_o \exp(E_a/kBT) \quad (1)$$

where σ_o is the pre-exponential factor, E_a is the activation energy, k_B is the Boltzmann's constant, and T is the absolute temperature. The activation energy of the conduction was estimated at 1 kHz from the slopes of the ln σ_{AC} versus $1/T$ curve. At 1 kHz, the calculated values of E_a were 0.51, 0.50, and 0.48 eV in the measured temperature range for CCTWO01, CCTWO03, and CCTWO05 ceramics, respectively.

Figure 7(b) shows the complex impedance spectrum (Z'' versus Z', Nyquist plot) of CCTWO01, CCTWO03, and CCTWO05 ceramics at 328 K. Complex plane impedance is powerful technique which separates the contributions of grains, grain boundaries, and electrode specimen interface to the total resistance and capacitance, respectively, by using the simplest equivalent RC circuit based on the brick-layer model.[59] It is observed from the Fig. 7(b) that the experimental impedance data only cover a part of the arcs, because of the limit of the measured frequency range. Only a fraction of the grain-boundary arc is observed in all the ceramics, composed of a resistor and capacitor joined in parallel. The doping of W affected the bulk (R_g) and grain-boundary (R_{gb}) resistance, and particularly for the grain

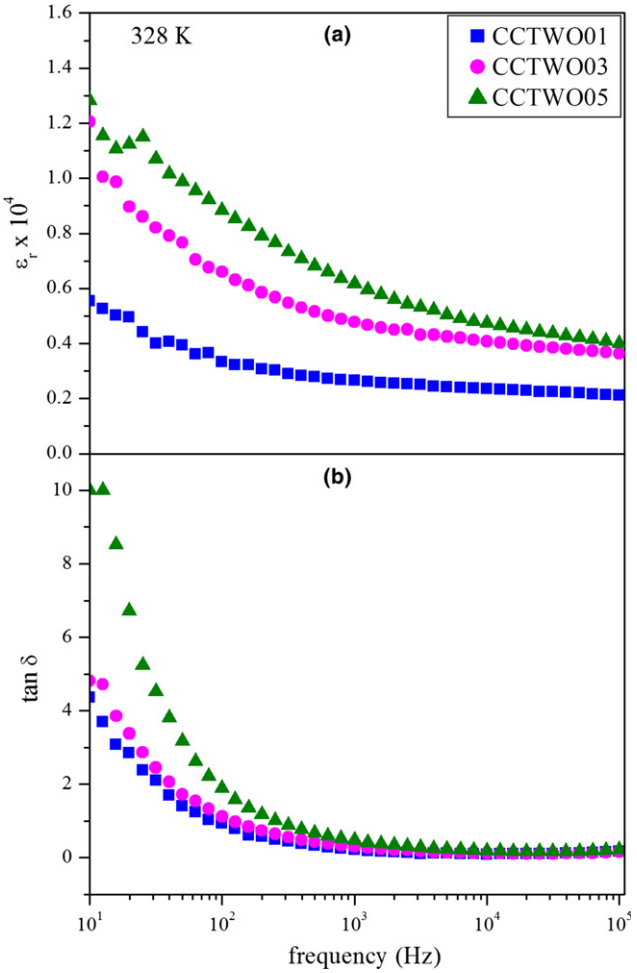

Fig. 6. Variations in (a) ε_r and (b) loss tangent (tan δ) vs. frequency at 328 K for the CCTWO01, CCTWO03, and CCTWO05 sintered at 1050°C for 30 h.

boundary. The values of the R_g and R_{gb} were obtained from the intercept of the Z' axis in the right (corresponding to the low frequency) is the R_{gb} and the intercept with the Z' axis in the left (corresponding to the high frequency) is R_g, as shown in the inset of Fig. 7(b). The values of the resistance can be calculated manually from the arc and listed in Table III, indicating that the R_g and R_{gb} decreased with increasing W concentration. This phenomenon indicates that W as the donor dopant affects the resistance of the R_g and R_{gb} by producing oxygen vacancies during the sintering process.[60] It is also suggested that the effective positive charge of W^{6+} in CCTO is compensated by the Ti vacancies and creation of conduction of electrons, which effect mainly on the potential barrier of GBs and responsible to decrease the values of R_{gb} and R_g. These results are consistent with the previously reported supervalent cations substitution in CCTO ceramic.[19,61]

Figures 8(a)–(c) show the variation in the imaginary part of the impedance Z'' with frequency for some representative temperatures of CCTWO01, CCTWO03, and CCTWO05. All the spectra are characterized by the appearance of a peak, shift in the peak position toward higher frequency, and typical peak broadening with increasing temperature, which behavior indicates the presence of a temperature-dependent electrical relaxation phenomenon in the ceramics. Similar type behavior has been reported for CCTO and other perovskites.[62, 63]

Figures 9(a)–(c) show the variation in the imaginary part of the electric modulus (M'') of the CCTWO01, CCTWO03, and CCTWO05 with frequency at different temperatures. All

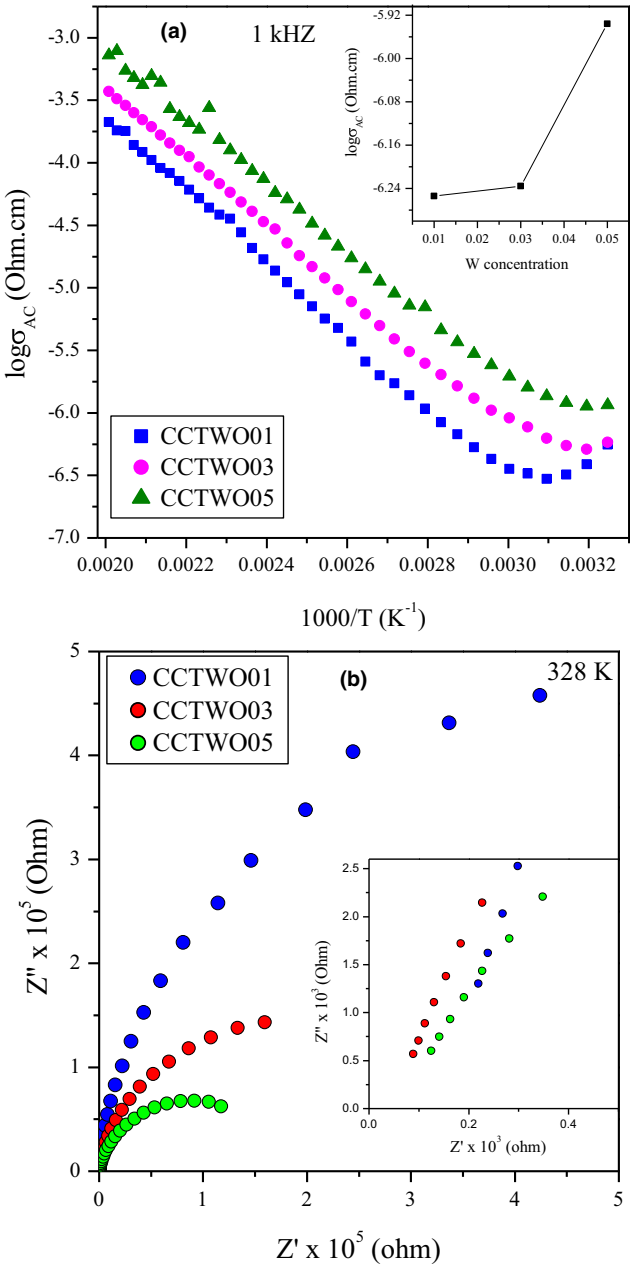

Fig. 7. (a) Plots of log σ_{AC} conductivity vs.1/T at 1 kHz: Inset shows the trend of conductivities at 308 K, at 1 kHz, and (b) impedance plane plots of Z" vs Z' at 328 K: Inset shows an expanded view of the high-frequency data close to the origin, for the CCTWO01, CCTWO03, and CCTWO05 sintered at 1050°C for 30 h.

Table III. Grain and Grain-Boundary Resistance for $CaCu_3Ti_{4-x}W_xO_{12}$ (x = 0.01, 0.03, and 0.05) at 328 K

	CCTWO01	CCTWO03	CCTWO05
R_g (Ω)	135.6	57.9	76.9
R_{gb} (Ω)	8.72×10^5	3.27×10^5	1.52×10^5

the ceramics exhibited asymmetric modulus peaks in the frequency range 10–10^5 Hz. The observed asymmetry in peak broadening indicates the spread of the relaxation time with different time constants, supporting the non-Debye type of relaxation present in the ceramics. The relaxation frequencies shifted toward higher frequencies with increasing peak height

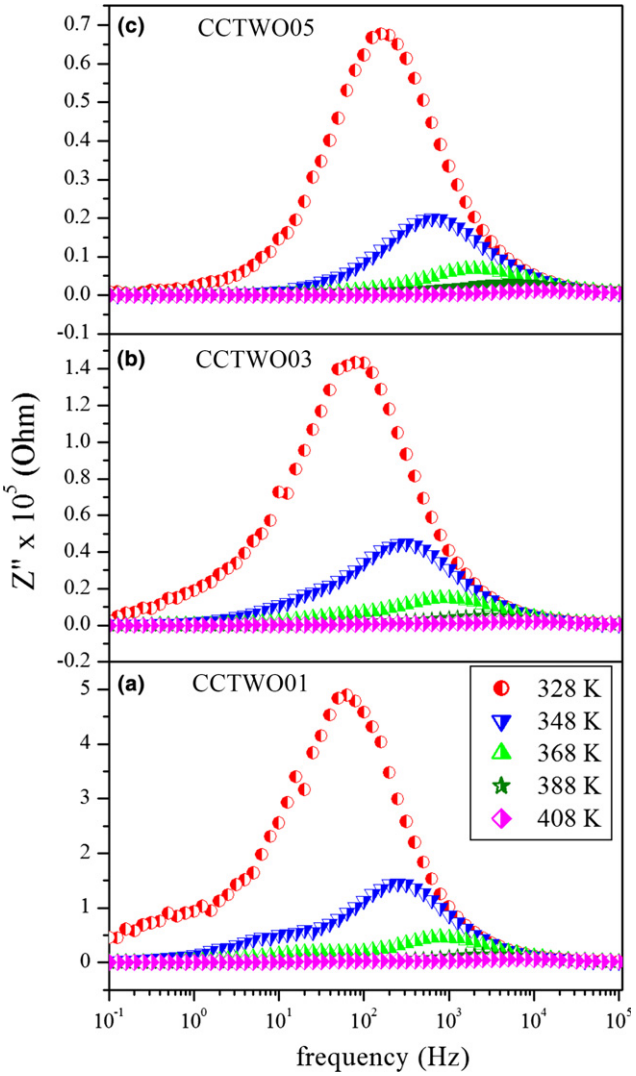

Fig. 8. Z" vs frequency at few selected temperatures for (a) CCTWO01, (b) CCTWO03, and (c) CCTWO05 sintered at 1050°C for 30 h.

and increasing temperature, indicating the thermally activated behavior of the relaxation time.

Figures 8 and 9 show the temperature-dependent relaxation phenomenon in the ceramics. For these ceramics, the most probable relaxation time (τ) for the grain boundaries relaxation was determined from the position of the relaxation peaks in the Z'' versus f (Fig. 8) and M'' versus f (Fig. 9). From these relaxation peaks, the relaxation frequency f was deduced, and then the relaxation time was calculated using the relation $\tau = 1/\omega = 1/2\pi f$, where ω is the angular frequency and f is the relaxation frequency. The τ value of these ceramics obeyed the Arrhenius linear relation.[64] As a result, the activation energy can be obtained by using the Arrhenius formula as shown in Eq. (2)

$$\tau = \tau_o \exp(E_a/k_B T) \quad (2)$$

where τ_o is the pre-exponential factor, E_a is the activation energy associated with the relaxation process, k_B is the Boltzmann's constant, and T is the absolute temperature.

Figures 10(a)–(c) show the nature of the variation in the relaxation time (τ) with the $1/T$ obtained from the impedance and modulus data of the CCTWO01, CCTWO03, and CCTWO05. The E_a values are calculated from the slope of ln τ versus $1/T$ plots of the impedance, and modulus data are

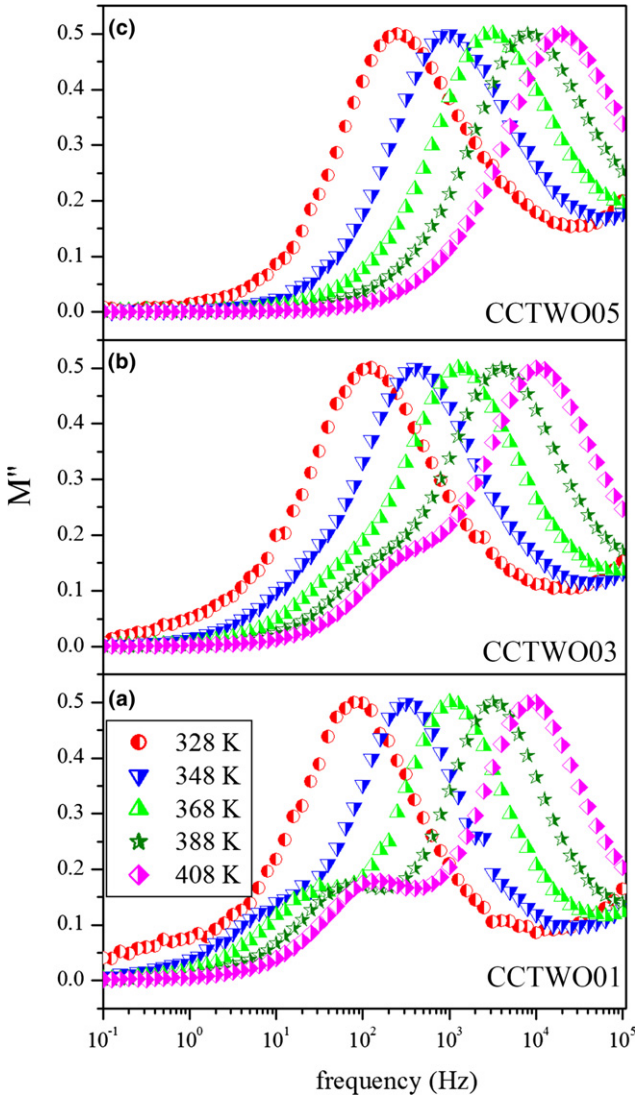

Fig. 9. Variation in the imaginary part of M" with frequency at different temperatures for (a) CCTWO01, (b) CCTWO03, and (c) CCTWO05 sintered at 1050°C for 30 h.

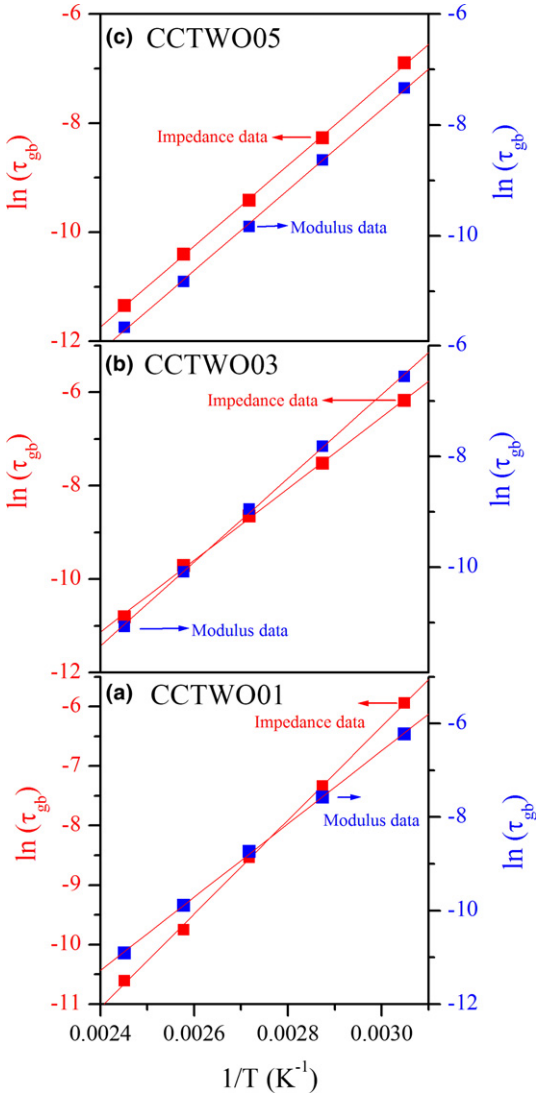

Fig. 10. Variation in τ deduced from the impedance and modulus data with inverse of temperature (1/T) for (a) CCTWO01, (b) CCTWO03, and (c) CCTWO05 sintered at 1050°C for 30 h.

listed in Table IV. These activation energies of the CCTWO ceramics are in close agreement with the values calculated for the grain-boundary contribution previously reported.[62]

IV. Conclusions

In this study, we investigated the dielectric properties of the $CaCu_3Ti_{4-x}W_xO_{12}$ (x = 0.01, 0.03, and 0.05) ceramics prepared by flame synthesis method. A major CCTO phase was obtained at 1050°C after 30 h, besides the minor phases of $CaTiO_3$ and CuO. The microstructures of the ceramics show that the average grain size was slightly increased with increasing W concentration. The dielectric property measurement shows that the ε_r and tan δ values in the measured frequency range at 328 K for W-doped ceramics were increased with increasing W content. The impedance and modulus analyses of these ceramics were proved to confirm the presence of the non-Debye type relaxation, which is temperature dependent.

Acknowledgments

This study was supported by the National Research Foundation (NRF-2015R1D1A3A01019167 for Y. Lee and NRF-2015R1D1A4A01019630 for L. Singh) and Priority Research Centers Program (NRF-2009-0093818) funded by the Ministry of Education in the Republic of Korea.

Table IV. E_a Values for Grain-Boundary Contribution Calculated from the ln τ versus $1/T$ from the Impedance and Modulus Data for $CaCu_3Ti_{4-x}W_xO_{12}$ (x = 0.01, 0.03, and 0.05)

	CCTWO01	CCTWO03	CCTWO05
E_a (eV) from Impedance	0.679	0.660	0.638
E_a (eV) from Modulus	0.674	0.651	0.625

References

[1]T. B. Adams, D. C. Sinclair, and A. R. West, "Influence of Processing Conditions on the Electrical Properties of $CaCu_3Ti_4O_{12}$ Ceramics," *J. Am. Ceram. Soc.*, **89**, 3129–35 (2006).

[2]D. L. West and D. A. Payne, "Microstructure Development in Reactive-Templated Grain Growth of Bi½Na½TiO$_3$-Based Ceramics: Template and Formulation Effects," *J. Am. Ceram. Soc.*, **86**, 769–74 (2003).

[3]T. Wang, L. Jin, C. Li, Q. Hu, and X. Wei, "Relaxor Ferroelectric $BaTiO_3$–$Bi(Mg_{2/3}Nb_{1/3})O_3$ Ceramics for Energy Storage Application," *J. Am. Ceram. Soc.*, **98**, 559–66 (2015).

[4]D. P. Shay, N. J. Podraza, N. J. Donnelly, and C. A. Randall, "High Energy Density, High Temperature Capacitors Utilizing Mn-Doped $0.8CaTiO_3$–$0.2CaHfO_3$ Ceramics," *J. Am. Ceram. Soc.*, **95**, 1348–55 (2012).

[5]M. A. Subramanian, D. Li, N. Duan, B. A. Reisner, and A. W. Sleight, "High Dielectric Constant in $ACu_3Ti_4O_{12}$ and $ACu_3Ti_3FeO_{12}$ Phases," *J. Solid State Chem.*, **151**, 323–5 (2000).

[6]A. P. Ramirez, et al., "Giant Dielectric Constant Response in a Copper-Titanate," *Solid State Comm.*, **115**, 217–20 (2000).
[7]L. Singh, U. S. Rai, K. D. Mandal, and N. B. Singh, "Progress in the Growth of $CaCu_3Ti_4O_{12}$ and Related Functional Dielectric Perovskites," *Prog. Crys. Growth Char. Mater.*, **60**, 15–62 (2014).
[8]T. T. Fang, J. W. Lin, and C. Y. Lin, "Evidence of the Ultrahigh Dielectric Constant of $CaSiO_3$-Doped $CaCu_3Ti_4O_{12}$ from Its Dielectric Response, Impedance Spectroscopy, and Microstructure," *Phys. Rev. B*, **76**, 045115–8 (2007).
[9]P. R. Bueno, W. C. Ribeiro, M. A. Ramirez, J. A. Varela, and E. Longo, "Separation of Dielectric and Space Charge Polarizations in $CaCu_3Ti_4O_{12}/CaTiO_3$ Composite Polycrystalline Systems," *Appl. Phys. Lett.*, **90**, 142912–3 (2007).
[10]L. Feng, X. Tang, Y. Yan, X. Chen, Z. Jiao, and G. Cao, "Decrease of Dielectric Loss in $CaCu_3Ti_4O_{12}$ Ceramics by La Doping," *Phys. Status Solid A*, **203**, R22–4 (2006).
[11]S. D. Hutagalung, L. Y. Ooi, and Z. A. Ahmad, "Improvement in Dielectric Properties of Zn-Doped $CaCu_3Ti_4O_{12}$ Electroceramics Prepared by Modified Mechanical Alloying Technique," *J. Alloy. Compd.*, **476**, 477–81 (2009).
[12]M. Li, A. Feteira, D. C. Sinclair, and A. R. West, "Influence of Mn Doping on the Semiconducting Properties of $CaCu_3Ti_4O_{12}$ Ceramics," *Appl. Phys. Lett.*, **88**, 232903–3 (2006).
[13]L. Ni and X. M. Chen, "Enhanced Giant Dielectric Response in Mg-Substituted $CaCu_3Ti_4O_{12}$ Ceramics," *Solid State Comm.*, **149**, 379–83 (2009).
[14]M. Li, G. Cai, D. F. Zhang, W. Y. Wang, W. J. Wang, and X. L. Chen, "Enhanced Dielectric Responses in Mg-Doped $CaCu_3Ti_4O_{12}$," *J. Appl. Phys.*, **104**, 074107–4 (2008).
[15]P. Leret, J. F. Fernandez, J. Frutos, and D. F. Hevia, "Nonlinear I–V Electrical Behavior of Doped $CaCu_3Ti_4O_{12}$ Ceramics," *J. Eur. Ceram. Soc.*, **27**, 3901–5 (2007).
[16]L. Singh, U. S. Rai, K. D. Mandal, and M. Yashpal, "Dielectric Properties of Ultrafine Zn-Doped $CaCu_3Ti_4O_{12}$ Ceramic," *J. Adv. Dielectr.*, **2**, 1250007–6 (2012).
[17]Q. Zheng, H. Fan, and C. Long, "Microstructures and Electrical Responses of Pure and Chromium-Doped $CaCu_3Ti_4O_{12}$ Ceramics," *J. Alloy. Compd.*, **511**, 90–4 (2012).
[18]M. A. Rubia, et al., "Dielectric Behavior of Hf-Doped $CaCu_3Ti_4O_{12}$ Ceramics Obtained by Conventional Synthesis and Reactive Sintering," *J. Eur. Ceram. Soc.*, **32**, 1691–9 (2012).
[19]M. A. Sulaimana, S. D. Hutagalung, M. F. Ain, and Z. A. Ahmad, "Dielectric Properties of Nb-Doped $CaCu_3Ti_4O_{12}$ Electroceramics Measured at High Frequencies," *J. Alloy. Compd.*, **493**, 486–92 (2010).
[20]P. Thongbai, J. Jumpatama, T. Yamwong, and S. Maensiri, "Effects of Ta^{5+} Doping on Microstructure Evolution, Dielectric Properties and Electrical Response in $CaCu_3Ti_4O_{12}$ Ceramics," *J. Eur. Ceram. Soc.*, **32**, 2423–30 (2012).
[21]Y. Liu, Q. Chen, and X. Zhao, "Dielectric Response of Sb-Doped $CaCu_3Ti_4O_{12}$ Ceramics," *J. Mater. Sci.: Mater. Electron.*, **25**, 1547–52 (2014).
[22]B. Barbier, et al., "$CaCu_3Ti_4O_{12}$ Ceramics from Co-Precipitation Method: Dielectric Properties of Pellets and Thick Films," *J. Eur. Ceram. Soc.*, **29**, 731–5 (2009).
[23]P. Jha, P. Arora, and A. K. Ganguli, "Polymeric Citrate Precursor Route to the Synthesis of the High Dielectric Constant Oxide, $CaCu_3Ti_4O_{12}$," *Mater. Lett.*, **57**, 2443–6 (2003).
[24]L. Singh, U. S. Rai, and K. D. Mandal, "Dielectric Properties of Zinc Doped Nanocrystalline Calcium Copper Titanate Synthesized by Different Approach," *Mater. Res. Bull.*, **48**, 2117–22 (2013).
[25]C. Masingbon, P. Thongbai, S. Maensiri, T. Yamwong, and S. Seraphin, "Synthesis and Giant Dielectric Behavior of $CaCu_3Ti_4O_{12}$ Ceramics Prepared by Polymerized Complex Method," *Mater. Chem. Phys.*, **109**, 262–70 (2008).
[26]R. Aoyagi, M. Iwata, and M. Maeda, "Effect of Sintering Temperature on the Dielectric Properties of $CaCu_3Ti_4O_{12}$ Ceramics," *Ferroelectrics*, **356**, 90–4 (2007).
[27]W. Q. Ni, X. H. Zheng, and J. C. Yu, "Sintering Effects on Structure and Dielectric Properties of Dielectrics $CaCu_3Ti_4O_{12}$," *J. Mater. Sci.*, **42**, 1037–41 (2007).
[28]L. Singh, U. S. Rai, K. D. Mandal, and A. K. Rai, "Sintering Effects on Dielectric Properties of Zn-Doped $CaCu_3Ti_4O_{12}$ Ceramic Synthesized by Modified Sol–Gel Route," *Elect. Mater. Lett.*, **9**, 107–13 (2013).
[29]A. Sutka and G. Mezinskis, "Sol–Gel Auto-Combustion Synthesis of Spinel-Type Ferrite Nanomaterials," *Front. Mater. Sci.*, **6**, 128–41 (2012).
[30]V. S. Puli, A. Kumar, D. B. Chrisey, M. Tomozawa, J. F. Scott, and R. S. Katiyar, "Barium Zirconate-Titanate/Barium Calcium-Titanate Ceramics via Sol–Gel Process: Novel High-Energy-Density Capacitors," *J. Phys. D: Appl. Phys.*, **44**, 395403–10 (2011).
[31]R. Schmidt, S. Pandey, P. Fiorenza, and D. C. Sinclair, "Non-Stoichiometry in $CaCu_3Ti_4O_{12}$ (CCTO) Ceramics," *RSC Adv.*, **3**, 14580–9 (2013).
[32]S. G. Fritsch, T. Lebey, M. Boulos, and B. Durand, "Dielectric Properties of $CaCu_3Ti_4O_{12}$ Based Multiphased Ceramics," *J. Eur. Ceram. Soc.*, **26**, 1245–57 (2006).
[33]Z. H. Ming, G. Y. Jun, L. Jian, Y. I. Danqing, and X. Lairong, "Microstructure and Mechanical Properties of 8YSZ Ceramics by Liquid-Phase Sintering with CuO-TiO_2 Addition," *J. Cent. South Univ.*, **19**, 1196–01 (2012).
[34]F. H. Lu, F. X. Fang, and Y. S. Chen, "Eutectic Reaction Between Copper Oxide and Titanium Dioxide," *J. Eur. Ceram. Soc.*, **21**, 1093–9 (2010).
[35]M. A. Rubia, J. J. Reinosa, P. Leret, J. J. Romero, J. de Frutos, and J. F. Fernández, "Experimental Determination of the Eutectic Temperature in Air of the CuO–TiO_2 Pseudobinary System," *J. Eur. Ceram. Soc.*, **32**, 71–6 (2012).
[36]W. X. Yuan, "Impedance and Electric Modulus Approaches to Investigate Four Origins of Giant Dielectric Constant in $CaCu_3Ti_4O_{12}$ Ceramics," *Solid State Sci.*, **14**, 330–4 (2012).
[37]L. T. Mei and H. I. Hsiang, "Effect of Copper-Rich Secondary Phase at the Grain Boundaries on the Varistor Properties of $CaCu_3Ti_4O_{12}$ Ceramics," *J. Am. Ceram. Soc.*, **91**, 3735–7 (2008).
[38]K. R. Reddy, et al., "A New One-Step Synthesis Method for Coating Multi-Walled Carbon Nanotubes with Cuprous Oxide Nanoparticles," *Scripta Mater.*, **58**, 1010–3 (2008).
[39]K. R. Reddy, V. G. Gomes, and M. Hassan, "Carbon Functionalized TiO_2 Nanofibers for High Efficiency Photocatalysis," *Mater. Res. Express*, **1**, 015012–5 (2014).
[40]K. R. Reddy, K. Nakata, T. Ochiai, T. Murakami, D. A. Tryk, and A. Fujishima, "Nanofibrous TiO_2-Core/Conjugated Polymer-Sheath Composites: Synthesis, Structural Properties and Photocatalytic Activity," *J. Nanosci. Nanotechnol.*, **10**, 7951–7 (2010).
[41]X. P. Wang, B. Q. Yang, H. X. Zhang, and P. X. Feng, "Tungsten Oxide Nanorods Array and Nanobundle Prepared by Using Chemical Vapor Deposition Technique," *Nanoscale Res. Lett.*, **2**, 405–9 (2007).
[42]O. Y. Khyzhun, "XPS, XES and XAS Studies of the Electronic Structure of Tungsten Oxides," *J. Alloy. Compd.*, **305**, 1–6 (2000).
[43]L. Singh, et al., "Dielectric Studies of a Nano-Crystalline $CaCu_{2.90}Zn_{0.10}Ti_4O_{12}$ Electro-Ceramic by One Pot Glycine Assisted Synthesis from Inexpensive TiO_2 for Energy Storage Capacitors," *RSC Adv.*, **4**, 52770–84 (2014).
[44]L. Singh, et al., "Comparative Dielectric Studies of Nanostructured $BaTiO_3$, $CaCu_3Ti_4O_{12}$ and $0.5BaTiO_3{\cdot}0.5CaCu_3Ti_4O_{12}$ Nano-Composites Synthesized by Modified Sol–Gel and Solid State Methods," *Mater. Character*, **96**, 54–62 (2014).
[45]L. F. Xu, P. B. Qi, S. S. Chen, R. L. Wang, and C. P. Yang, "Dielectric Properties of Bismuth Doped $CaCu_3Ti_4O_{12}$ Ceramics," *Mater. Sci. Eng., B*, **177**, 494–8 (2012).
[46]A. R. West, T. B. Adams, F. D. Morrison, and D. C. Sinclair, "Novel High Capacitance Materials:- $BaTiO_3$:La and $CaCu_3Ti_4O_{12}$," *J. Eur. Ceram. Soc.*, **24**, 1439–48 (2004).
[47]L. Singh, U. S. Rai, and K. D. Mandal, "Dielectric, Modulus and Impedance Spectroscopic Studies of Nanostructured $CaCu_{2.70}Mg_{0.30}Ti_4O_{12}$ Electro-Ceramic Synthesized by Modified Sol–Gel Route," *J. Alloy. Compd.*, **555**, 176–83 (2013).
[48]J. Li, P. Liang, J. Yi, X. Chao, and Z. Yang, "Phase Formation and Enhanced Dielectric Response of $Y_{2/3}Cu_3Ti_4O_{12}$ Ceramics Derived from the Sol–Gel Process," *J. Am. Ceram. Soc.*, **1**, 1–9 (2014).
[49]L. Singh, U. S. Rai, K. D. Mandal, B. C. Sin, S. I. Lee, and Y. Lee, "Dielectric, AC-Impedance, Modulus Studies on $0.5BaTiO_3{\cdot}0.5CaCu_3Ti_4O_{12}$ Nano-Composite Ceramic Synthesized by One-Pot, Glycine-Assisted Nitrate-Gel Route," *Ceram. Int.*, **40**, 10073–83 (2014).
[50]K. R. Reddy, H. M. Jeong, Y. Lee, and A. V. Rahhu, "Synthesis of MWCNTs-Core/Thiophene Polymer-Sheath Composite Nanocables by a Cationic Surfactant-Assisted Chemical Oxidative Polymerization and Their Structural Properties," *J. Polym. Sci. A Polym. Chem.*, **48**, 1477–84 (2010).
[51]K. R. Reddy, B. C. Sin, K. S. Ryu, J. Noh, and Y. Lee, "*In Situ* Self-Organization of Carbon Black–Polyaniline Composites from Nanospheres to Nanorods: Synthesis, Morphology, Structure and Electrical Conductivity," *Syn. Met.*, **159**, 1934–9 (2009).
[52]K. R. Reddy, B. C. Sin, C. H. Yoo, D. Sohn, and Y. Lee, "Coating of Multiwalled Carbon Nanotubes with Polymer Nanospheres Through Microemulsion Polymerization," *J. Colloid Interface Sci.*, **340**, 160–5 (2009).
[53]K. R. Reddy, B. C. Sin, K. S. Ryu, J. C. Kim, H. Chung, and Y. Lee, "Conducting Polymer Functionalized Multi-Walled Carbon Nanotubes with Noble Metal Nanoparticles: Synthesis, Morphological Characteristics and Electrical Properties," *Syn. Met.*, **159**, 595–603 (2009).
[54]K. R. Reddy, W. Park, B. C. Sin, J. Noh, and Y. Lee, "Synthesis of Electrically Conductive and Superparamagnetic Monodispersed Iron Oxide-Conjugated Polymer Composite Nanoparticles by *In Situ* Chemical Oxidative Polymerization," *J. Colloid Interface Sci.*, **335**, 34–9 (2009).
[55]K. R. Reddy, K. P. Lee, and A. I. Gopalan, "Self-Assembly Approach for the Synthesis of Electro-Magnetic Functionalized Fe_3O_4/Polyaniline Nanocomposites: Effect of Dopant on the Properties," *Colloids Surf. A*, **320**, 49–56 (2008).
[56]Y. P. Zhang, S. H. Lee, K. R. Reddy, A. I. Gopalan, and K. P. Lee, "Synthesis and Characterization of Core-Shell SiO_2 Nanoparticles/Poly(3-Aminophenylboronic Acid) Composites," *J. Appl. Polym. Sci.*, **104**, 2743–50 (2007).
[57]K. R. Reddy, K. P. Lee, Y. Lee, and A. I. Gopalan, "Facile Synthesis of Conducting Polymer–Metal Hybrid Nanocomposite by in Situ Chemical Oxidative Polymerization with Negatively Charged Metal Nanoparticles," *Mater. Lett.*, **62**, 1815–8 (2008).
[58]Y. Liu, W. Wang, J. Huang, F. Tang, C. Zhu, and Y. Cao, "Dielectric Properties of Giant Permittivity $NaCu_3Ti_3NbO_{12}$ Ceramics," *Ceram. Int.*, **39**, 9201–6 (2013).
[59]A. K. Behera, N. K. Mohanty, B. Behera, and P. Nayak, "Impedance Properties of $0.7(BiFeO_3)$-$0.3(PbTiO_3)$ Composite," *Adv. Mat. Lett.*, **4**, 141–5 (2013).
[60]B. S. Prakash and K. B. R. Varma, "Microstructural and Dielectric Properties of Donor Doped (La^{3+}) $CaCu_3Ti_4O_{12}$ Ceramics," *J. Mater. Sci.: Mater. Electron.*, **17**, 899–907 (2006).
[61]S. Y. Chung, J. H. Choi, and J. K. Choi, "Tunable Current-Voltage Characteristics in Polycrystalline Calcium Copper Titanate," *Appl. Phys. Lett.*, **91**, 091912–3 (2007).
[62]S. Y. Lee, Y. W. Hong, and S. I. Yoo, "Dielectric Properties of $CaCu_3Ti_4O_{12}$ Polycrystalline Ceramics," *Elect. Mater. Lett.*, **7**, 287–96 (2013).
[63]P. Liang, X. Chao, and Z. Yang, "Low Dielectric Loss, Dielectric Response, and Conduction Behavior in Na-Doped $Y_{2/3}Cu_3Ti_4O_{12}$ Ceramics," *J. Appl. Phys.*, **116**, 044101–9 (2014).
[64]D. K. Mahato, A. Dutta, and T. P. Sinha, "Impedance Spectroscopy Analysis of Double Perovskite Ho_2NiTiO_6," *J. Mater. Sci.*, **45**, 6757–62 (2010). □